CERN-TH. 6350/91
DESY 91/140
ETH-TH-91/43
LMU-91/05

Signals of New Gauge Bosons at Future e^+e^- Colliders

A. Djouadi[1], **A. Leike**[2,3,*], **T. Riemann**[3,4], **D. Schaile**[5] and **C. Verzegnassi**[6,†]

[1] Deutsches Electronen Synchrotron, DESY, W–2000 Hamburg 52, Germany

[2] Ludwig–Maximilians–Universität, Section Physik, W–8000 Munich, Germany

[3] Institut für Hochenergiephysik, O–1615 Zeuthen, Germany

[4] Theory Division, CERN, CH–1211 Geneva 23, Switzerland

[5] Fakultät für Physik, Albert–Ludwigs–Universität, W–7800 Freiburg, Germany

[6] Theoretical Physics Institute, ETH, Zurich, Switzerland

ABSTRACT

We analyze possible indirect signals of additional neutral gauge bosons at future e^+e^- colliders, concentrating on $SU(2)_L \times U(1)_Y \times U(1)_{Y'}$ and $SU(2)_L \times SU(2)_R \times U(1)$ effective theories. We develop a simple formalism to describe these effects and make a careful study of radiative corrections, in particular initial state radiation, which will be shown to have important implications. To make realistic estimates of the sensitivity to the new gauge boson effects, we use a model detector for e^+e^- annihilation at a center of mass energy of 500 GeV. Using a number of selected physical observables we then show that masses considerably higher than the total energy [up to a factor of 6] can be probed and that distinction between various theoretical models is possible.

CERN-TH. 6350/91
December 1991

*Supported in part by the Alexander von Humboldt - Stiftung

†On leave of absence from Dept. of Theoretical Physics, Trieste, and INFN, Sezione di Trieste

1 Introduction

The Standard Model of strong and electroweak interactions [1], based on the gauge symmetry $SU(3)_C \times SU(2)_L \times U(1)_Y$, has achieved many successes in describing the experimental data within the range of energies available today. In particular, it has been tested to the level of its loop radiative corrections in the high precision LEP experiments. Nevertheless, it is widely believed that it is not the ultimate truth. Indeed, besides the fact that it has too many parameters which are merely incorporated by hand, it does not unify the electromagnetic, weak and strong forces in a satisfactory way since the coupling constants of the three gauge groups are different and independent. Therefore, one would expect the existence of a more fundamental theory in which the Standard Model is naturally embedded and which reduces to it at present energies.

Among the candidates for this more fundamental picture, grand unified theories are the most appealing ones. Not only do they unify electroweak and strong interactions within the context of a single gauge group but they also, when endowed with supersymmetry, lead to a successful prediction for the coupling constants of these interactions at low energies [2]. In particular, the exceptional group E_6 [3], which contains the popular subgroups SU(5) [4] and SO(10) [5] and is the next simple anomaly free choice after SO(10), has received most of the attention in recent years [6]. This is mainly due to the fact that superstring theories, which attempt to unify all fundamental forces including gravity, suggest that this symmetry is an acceptable four dimensional field theoretic limit after compactification [7].

A general prediction of grand unified theories [with the notable exception of the one based on SU(5) symmetry] is the existence of additional gauge bosons [3, 5, 6]. Indeed, in the breaking of these symmetries down to the Standard Model gauge group, it is possible that some additional group factors survive at low energies, allowing for at least one extra neutral gauge boson [to be generically called Z' from now on] with a mass not far from the scale of the electroweak symmetry breaking. This additional boson could then be light enough to generate observable effects at the next generation of electron–positron or hadron colliders.

At hadron colliders, the direct production of new bosons has been extensively studied by several groups [see ref.[6] for a compilation and references therein]. Depending on the assumed luminosity of the machine, the nature of the Z' as well as its decay branching fractions, discovery limits range up to 3–5 TeV at the LHC [8] and up to 5–6 TeV at the SSC [9]. In principle, it might also be possible to identify the physical origin of the Z' [at least within classes of models] using the leptonic forward–backward asymmetry. However, because of experimental difficulties this will not be possible for the entire discovery range and for instance at the LHC, it would probably be limited to Z' masses below 1 TeV [8].

At the next linear e^+e^- colliders, since their presently planned energies do not exceed one TeV, the possibility of directly producing a new gauge boson is more limited than at LHC/SSC. However, even if a new Z' is too heavy to be produced as a resonance, it could give rise to virtual effects which are measurable. As a matter of fact, due to the clean environment of e^+e^- annihilation, high precision measurements can be performed and masses

considerably higher than the maximum center of mass energy can be probed. In addition, because of the much larger number of experimental observables which can be measured with a high accuracy, the possibility of identifying the model origin of the new gauge boson is not as limited as in the case of hadron colliders. For instance if a Z' with a mass of the order of 1–2 TeV is found at the LHC, a 500 GeV e^+e^- collider would give valuable contributions to its detailed investigation, allowing the distinction between different models and the determination of the model parameters. The study of the effects of the new gauge boson at hadron and e^+e^- colliders would then be complementary.

In the present article, we shall study the possible effects of one extra neutral gauge boson at high energy e^+e^- colliders, concentrating on two general effective theories: $\mathrm{SU(2)_L} \times \mathrm{U(1)_Y} \times \mathrm{U(1)_{Y'}}$ originating from the $\mathrm{E_6}$ model and left–right models [10] based on an $\mathrm{SU(2)_L} \times \mathrm{SU(2)_R} \times \mathrm{U(1)}$ symmetry. We shall assume that the new boson will be heavier than the total energy of the collider so that it can reveal its existence only through virtual effects which could be measurable in a high precision experiment. Several preliminary studies of the subject have been conducted in recent years [11, 12] and search "strategies" have been developed to isolate the signals of the Z' and to identify its model origin. However, there are some important aspects of these indirect searches via high precision measurements which have not been considered previously, and which we shall discuss in detail.

In previous analyses, the indirect effects of new bosons on physical observables were studied in the Born approximation and radiative corrections have been generally ignored. However, since far below the production threshold the Z' effects on measurable quantities are expected to be rather small [and to have no special signature], one has to ensure that the latter quantities are calculated with the requested accuracy and therefore to incorporate both electroweak and QED radiative corrections. While the contributions of the weak loop corrections will only change the overall normalization, the photonic corrections and in particular initial state radiation give very large contributions which depend on the experimental conditions. Therefore, for a realistic analysis of indirect effects, these radiative corrections and their dependence on the experimental set–up must be carefully taken into account.

Another important question that we want to address in this paper is related to the experimental conditions under which the search of the virtual effects is made. The range of Z' masses and couplings which can be probed at an e^+e^- collider will directly depend on the experimental errors with which the physical observables are measured. Hence, one has to make realistic estimates of these errors in order to be able to select those observables which are the most sensitive to the new effects and best suited to probe higher masses and differentiate between various models. In addition one has to carefully control the potential "backgrounds" to the selected quantities by using suitable experimental cuts. These cuts have to be made in conjunction with those needed to control initial state radiation and hence must be optimized.

We shall also present a very convenient formalism to parametrize the virtual effects of extra neutral gauge bosons on various cross sections and [unpolarized as well as polarized] asymmetries in the annihilation process of the initial electron–positron pair to fermion pairs. The latter observables will be expressed with the help of generalized charges which are given in

terms of helicity amplitudes. Exact and compact formulae, including the final fermion mass effects which can be useful in the case of the third generation quarks, will be given.

Since some experimental conditions must be specified in order to make quantitative predictions, we will concentrate our analysis on the specific case of the Next Linear Collider (NLC) with a center of mass energy of 500 GeV. To make the study as realistic as possible, we will exploit the various studies which have been recently done on the potential of this machine [13, 14]. However, our results can be easily translated to higher [or smaller as it is the case for LEP200] energies by a proper reconsideration of the experimental situation. For the most important features, examples for different energies will be given.

The paper is organized as follows. The next section is devoted to the discussion of the main features of the $\mathrm{SU(2)_L \times U(1)_Y \times U(1)_{Y'}}$ and $\mathrm{SU(2)_L \times SU(2)_R \times U(1)}$ effective models which will be considered. We summarize the available information on the new parameters that are introduced and show how they affect the various observables used in our analysis. In section 3, we discuss the rôle of pure electroweak and QED radiative corrections in the search for indirect effects and show how the radiative tail of the Z boson can be controlled. In the following section, we summarize the experimental situation of e^+e^- annihilation at a center of mass energy of 500 GeV. Extrapolating from the present knowledge, we use a realistic model detector to estimate the possible experimental accuracy on the observables that we select for the Z' search. Section 5 contains ours results. We exhibit the 95% confidence level range of masses and couplings that can be explored at the 500 GeV collider and study the possibility of distinguishing between various models with and without beam polarization. In the final section 6 we will summarize our main results and draw some conclusions. In the Appendix we collect the compact expressions of all the observables which are used for this search.

2 Theoretical Models

We will concentrate our attention on two of the most theoretically motivated effective theories which lead to an additional gauge boson Z' : $\mathrm{SU(2)_L \times U(1)_Y \times U(1)_{Y'}}$ originating from the breaking of the exceptional group $\mathrm{E_6}$ and left–right (LR) models based on an $\mathrm{SU(2)_L \times SU(2)_R \times U(1)}$ symmetry. In this section we discuss the main features of these two models, give the formalism needed to describe the effects of the Z', and summarize the available constraints on the new parameters.

In the breaking of the $\mathrm{E_6}$ group down to the Standard Model, two additional neutral gauge bosons will appear but for simplicity we assume that only one of them is light enough to be relevant. Its most general couplings can be conveniently parametrized in terms of the $\mathrm{U(1)_\psi}$ and $\mathrm{U(1)_\chi}$ charges where the U(1) factors result from the breaking of $\mathrm{E_6}$ via the chain [we follow the notations of [12]]

$$E_6 \longrightarrow SO(10) \times U(1)_\psi \longrightarrow SU(5) \times U(1)_\chi \times U(1)_\psi$$

The most general $Z^{0'}$ of this origin will be defined as

$$Z^{0'} \;=\; Z_\chi^{0'} \cos\beta + Z_\psi^{0'} \sin\beta \tag{1}$$

In this case the values $\beta = 0$ and $\beta = \pi/2$ would correspond to pure $Z_\chi^{0'}$ and $Z_\psi^{0'}$ gauge bosons respectively, while the choice $\beta = \mathrm{arctg}(-\sqrt{3/5})$ would correspond to the model η where E_6 is directly broken to a rank–5 group at the unification scale in superstrings theories. In the presence of this additional gauge boson, the neutral current Lagrangian will be given [in the weak eigenstate basis] by

$$\mathcal{L}_{\rm NC} = e J_\gamma^\mu A_\mu \;+\; g_Z J_Z^\mu Z_\mu^0 \;+\; g_{Z'} J_{Z'}^\mu Z_\mu^{0'} \tag{2}$$

where $e = \sqrt{4\pi\alpha}$, $g_Z = e/s_W c_W$, $g_{Z'} = e/c_W$ [with $s_W^2 = 1 - c_W^2 \equiv \sin^2\theta_W$] are the gauge coupling constants; we have assumed $g_Y = g_{Y'}$. The currents are [the sum runs over fermions]

$$J_V^\mu = \sum_f \overline{\psi}_f \gamma^\mu \left[\; Q_L^{fV} \; \frac{(1-\gamma_5)}{2} \;+\; Q_R^{fV} \; \frac{(1+\gamma_5)}{2} \; \right] \psi_f \tag{3}$$

with $V \equiv \gamma$, Z or Z' and $Q_{L,R}^{fV}$ their reduced left–handed and right-handed couplings to the fermions which are displayed in Table 1. In the case of the photon and Z boson, they are simply given by [e_f is the electric charge in units of e and I_{3L}^f is the third component of the weak isospin]

$$\begin{aligned} Q_L^{f\gamma} &= e^f \quad , & Q_R^{f\gamma} &= e^f \\ Q_L^{fZ} &= I_{3L}^f - e^f s_W^2 \quad , & Q_R^{fZ} &= -e^f s_W^2 \end{aligned} \tag{4}$$

The physical [mass eigenstates] Z and Z' are admixtures of the weak eigenstates Z^0 of SU(2) $\times$U(1) and $Z^{0'}$ of the additional U(1). The matrix describing this mixing is

$$\begin{pmatrix} Z \\ Z' \end{pmatrix} = \begin{pmatrix} \cos\theta_{\rm mix} & \sin\theta_{\rm mix} \\ -\sin\theta_{\rm mix} & \cos\theta_{\rm mix} \end{pmatrix} \begin{pmatrix} Z^0 \\ Z^{0'} \end{pmatrix}$$

where the angle $\theta_{\rm mix}$ is approximately given by the following expression [valid for $M_{Z'}$ sufficiently larger than M_Z]

$$\theta_{\rm mix} \simeq -s_W \frac{\sum_i v_i^2 \; I_{3L}^i \; Q_i'}{\sum_i v_i^2 \; (I_{3L}^i)^2} = P \; \frac{M_Z^2}{M_{Z'}^2} \tag{5}$$

where v_i are the vacuum expectation values of the (doublet) Higgs fields involved in the symmetry breaking and Q_i their charges with respect to the additional U(1). In most of the models which have been considered so far in the literature the parameter P is of the order of unity. This mixing between the Z and the Z' will induce a change in the couplings of the two bosons to fermions[1] from the values given in eq. (3); and can be straightforwardly included by performing the following substitutions

$$\begin{aligned} Q_{L,R}^{fZ} &\longrightarrow \; Q_{L,R}^{fZ} \cos\theta_{\rm mix} + s_W Q_{L,R}^{fZ'} \sin\theta_{\rm mix} \\ Q_{L,R}^{fZ'} &\longrightarrow \; -\frac{1}{s_W} Q_{L,R}^{fZ} \sin\theta_{\rm mix} + Q_{L,R}^{fZ'} \cos\theta_{\rm mix} \end{aligned} \tag{6}$$

[1]Note that the E_6 model predicts also the existence of new fermions [to complete the representation of dimension **27** of the group] which can mix with the standard ones [6]. These new fermions and their mixing will not be considered here.

Because the couplings of the Z boson to ordinary fermions have been very accurately measured at LEP100 and have been found to be in a very good agreement with the Standard Model expectations, the mixing angle is constrained to be rather small. Several analyses of the LEP100 data have reached at the conclusion that $\theta_{\rm mix}$ should be smaller than a few percent [15, 16]. This constraint will be more stringent in the future [17]. Hence, one can safely neglect its effects in the present analysis.

Since there is a strong correlation between the mixing angle $\theta_{\rm mix}$ and the Z' mass $M_{Z'}$ as shown in eq. (5), the constraint on $\theta_{\rm mix}$ directly translates into a lower bound on $M_{Z'}$, once the Higgs structure of the model is specified. Since in most of the theoretically well motivated models the parameter P is of the order of unity, one is led to a lower bound of several hundred[2] GeV on $M_{Z'}$. In addition to these indirect limits, lower bounds on $M_{Z'}$ from direct Z' searches at present hadron colliders are also available. From the negative search of a peak in the invariant mass spectrum of high energy e^+e^- pairs at the Tevatron, an area in the plane $M_{Z'}$ and Br($Z' \to e^+e^-$) has been excluded. Depending on the particular model chosen, extra neutral bosons with masses less than 200 to 400 GeV are already ruled out [15]. The accessible Z' mass range will probably be pushed up to $\sim$ 500 GeV in the next runs.

In the case of left–right models, following the notation of ref.[19], the most general $Z^{0'}_{LR}$ boson will couple to the current

$$J^\mu_{LR} \;=\; \alpha_{LR} J^\mu_{3R} - \frac{1}{2\alpha_{LR}} J^\mu_{B-L} \tag{7}$$

where J_{3R} is the current associated to the third component of the SU(2)$_R$ group, B and L are the baryon and lepton numbers respectively, and the model parameter α_{LR} is defined as

$$\alpha_{LR} \equiv \sqrt{\frac{c^2_W}{s^2_W}\frac{g^2_R}{g^2_L} - 1} \tag{8}$$

with $g_L = e/s_W$ and g_R being the SU(2)$_L$ and SU(2)$_R$ gauge coupling constants. The parameter α_{LR} will be restricted to lie in the range $\sqrt{2/3} \leq \alpha_{LR} \leq \sqrt{2}$. The upper bound corresponds to a left–right symmetric model $g_R = g_L$. When α_{LR} is equal to its lower bound, the LR model becomes identical to the χ model of E$_6$. This is due to the fact that SU(2)$_L$ $\times$ SU(2)$_R$ $\times$ U(1) can be generated by SO(10). From the existing analyses, mixing angles larger than 1% and Z'_{LR} masses smaller than $\sim$ 300 GeV are already ruled out by the available data [15, 16]. The experimental data on the charged current sector are much more constraining [20] and this sector can be safely ignored in our analysis.

An additional Z' would participate in the annihilation process $e^+e^- \to$ fermions[3] which will be built–up by a superposition of gauge boson s–channel exchanges [in the case of final

[2]However, this bound can be evaded in some models where P is very small or exactly vanishing [as it happens for instance in the case where tg$\beta = \sqrt{3/5}$], therefore generating a "spontaneous decoupling" of the Z' boson [18] from LEP physics and allowing its mass to be relatively small.

[3]We will not discuss the case of W boson pair production since the cross section is suppressed by mixing angle factors.

state electrons one also has t–channel exchanges]. Thus, it will alter the reaction through its propagator effects. For a heavy Z' the $\gamma Z'$ and ZZ' interferences should dominate over the $Z'Z'$ contribution. Furthermore the couplings of the photon to fermions are generally larger than those of the Z so that the largest contribution will be due to the $\gamma Z'$ interference term if the vectorial couplings of the Z' are not suppressed. The most general form of the differential cross section of the process $e^+e^- \to f\bar{f}$ is given in the Appendix, assuming initial [longitudinal or transverse] polarization of the beams and taking into account the masses of the final particles. This form is very convenient for practical purposes. Compact analytic expressions for the cross sections and for various observables which can be built–up in e^+e^- collisions are also given in the Appendix.

3 Radiative Corrections

Since the effects of heavy new gauge bosons [with masses far beyond the production threshold] on physical observables are expected to be rather small, in order to isolate new signals from standard effects one has to calculate the various contributions to these observables with the maximum accuracy. Hence, one has to properly take into account QED, pure weak and QCD radiative corrections. In particular, the QED bremsstrahlung corrections which depend on the experimental conditions, can give very large contributions. This is illustrated in Figure 1 where we display the total cross section for muon pair production in the presence of a Z' of mass $M_{Z'} = 700$ GeV, as a function of the center of mass energy. The largest contribution is due to initial state radiation, but our numerical results [21] also include final state radiation and the interference between initial and final state bremsstrahlung. Because the latter two corrections are numerically small we will not discuss them here[4]. In the following, we shall simply give the necessary formalism needed to include initial state bremsstrahlung and make few comments on pure weak and QCD radiative corrections.

The initial state corrected cross sections and forward–backward asymmetries can be obtained by using the following convolution formulae:

$$\sigma_T = \int_0^\Delta dk\ \sigma_T^0(s')\ R_T^e(k) \tag{9}$$

$$A_{FB} = \frac{1}{\sigma_T}\int_0^\Delta dk\ \sigma_{FB}^0(s')\ R_{FB}^e(k) \tag{10}$$

To first order in α, improved by soft photon exponentiation, the two functions R_T^e [23] and R_{FB}^e [24] are given by the following expressions

$$R_{T,FB}^e(k) = (1+S_e)\beta_e k^{\beta_e - 1}\ +\ H_{T,FB}^e(k) \tag{11}$$

where $\beta_e = 2\frac{\alpha}{\pi}e_e^2(\ln s/m_e^2 - 1)$ and S_e, $H_{T,FB}^e(k)$ are the soft and hard radiator parts

$$S_e\ =\ \frac{\alpha}{\pi}e_e^2\left[\frac{\pi^2}{3} - \frac{1}{2} + \frac{3}{2}(\ln\frac{s}{m_e^2} - 1)\right]$$

[4]These two sets of corrections are simple adaptations of known formulae from the standard theory. For a detailed discussion see ref.[22].

$$
\begin{aligned}
H_T(k) &= \frac{\alpha}{\pi} e_e^2 \left\{ \frac{1+(1-k)^2}{k} \left(\ln \frac{s}{m_e^2} - 1 \right) \right\} - \frac{\beta_e}{k} \\
H_{FB}(k) &= \frac{\alpha}{\pi} e_e^2 \left\{ \frac{1+(1-k)^2}{k} \frac{1-k}{(1-k/2)^2} \left(\ln \frac{s}{m_e^2} - 1 - \ln \frac{1-k}{(1-k/2)^2} \right) \right\} - \frac{\beta_e}{k}
\end{aligned}
\tag{12}
$$

Soft photons are radiated isotropically and as a consequence, $R^e_{T,FB}(k \to 0)$. Since at the Z boson peak soft photon emission is dominating, the difference of the radiators for σ_T and σ_{FB} may be neglected at LEP100. This is no longer true for energies sufficiently above this narrow resonance. In eqs.(9–10), $\sigma^0_{T,FB}$ are the Born cross sections taken at a reduced energy $s' = s(1-k)$. In the massless fermion case [the exact expressions including mass effects are given in the Appendix] they read

$$
\sigma^0_T = \frac{4}{3} \frac{\pi\alpha^2}{s'} \Re e \sum_{m,n=0}^{2} \left[Q_T^{m,n} (1 - P_L^+ P_L^-) + Q_{FB}^{m,n} (P_L^+ - P_L^-) \right] \chi_m(s') \chi_n^*(s') \tag{13}
$$

$$
\sigma^0_{FB} = \frac{\pi\alpha^2}{s'} \Re e \sum_{m,n=0}^{2} \left[Q_{FB}^{m,n} (1 - P_L^+ P_L^-) + Q_T^{m,n} (P_L^+ - P_L^-) \right] \chi_m(s') \chi_n^*(s') \tag{14}
$$

where $\alpha \equiv \alpha(s')$ is the running electromagnetic constant, $P_L^\pm$ are the longitudinal polarizations of $e^\pm$ and m, n denote the three gauge bosons γ, Z, Z' with propagators

$$
\begin{aligned}
\chi_0(s) &= \frac{s}{s - m_0^2} \quad \text{with} \quad m_0^2 = 0 \quad \text{for} \quad \gamma \\
\chi_1(s) &= \frac{\xi}{s_W^2 c_W^2} \frac{s}{s - m_1^2} \quad \text{with} \quad m_1^2 = M_Z^2 - i M_Z \Gamma_Z \quad \text{for} \quad Z \\
\chi_2(s) &= \frac{1}{c_W^2} \frac{s}{s - m_2^2} \quad \text{with} \quad m_2^2 = M_{Z'}^2 - i M_{Z'} \Gamma_{Z'} \quad \text{for} \quad Z'
\end{aligned}
$$

Here $\xi, \xi = \sqrt{2} G_F M_W^2 s_W^2 / \pi\alpha \sim 1$, is introduced to take into account additional electroweak corrections which improve the Born approximation. In terms of the fermion charges $Q^{fV}_{L,R}$ given in Table 1, Q_T and Q_{FB} are

$$
\begin{aligned}
Q_T^{m,n} &= \frac{1}{4} \left[Q_L^{em} Q_L^{en} + Q_R^{em} Q_R^{en} \right] \times \left[Q_L^{fm} Q_L^{fn} + Q_R^{fm} Q_R^{fn} \right] \\
Q_{FB}^{m,n} &= \frac{1}{4} \left[Q_L^{em} Q_L^{en} - Q_R^{em} Q_R^{en} \right] \times \left[Q_L^{fm} Q_L^{fn} - Q_R^{fm} Q_R^{fn} \right]
\end{aligned}
\tag{15}
$$

The result of the integration of eqs.(9–10) are analytic functions depending on the exchanged boson mass and couplings and the cut Δ on the photon energy. We have chosen a simple parametrization of the photon phase space which nevertheless allows to exhibit the essential features of a more realistic experimental set-up. We come now to the discussion of the development of the radiative tail. The product of the propagators in eqs.(13-14) can be written as

$$
\frac{s'}{s' - m_m^2} \frac{s'}{s' - m_n^{*2}} = \frac{s}{m_n^{*2} - m_m^2} \frac{s'}{s} \left[\frac{s'}{s' - m_n^{*2}} - \frac{s'}{s' - m_m^2} \right] \tag{16}
$$

and in the case where $m = n$, one has for the first factor on the right–hand side

$$\frac{s}{m_m^{*2} - m_m^2} \;=\; \frac{i}{2}\frac{M_m}{\Gamma_m}\frac{s}{M_m^2} \tag{17}$$

This imaginary number is a quantitative measure of the radiative tail. It gives real contributions to the cross section if it is met by another imaginary quantity, which can arise from the integration over the other [s'–dependent] factors in eq. (16). After partial fraction decomposition, one arrives at

$$\frac{i}{2}\;\frac{s}{M_m^2}\frac{M_m}{\Gamma_m}\;\int_0^\Delta\; dk\;\frac{1}{(1-k) - m_m^2/s} \;=\; \frac{i}{2}\;\frac{s}{M_m^2}\;\frac{M_m}{\Gamma_m}\;\ln\frac{\Delta - 1 + m_m^2/s}{-1 + m_m^2/s} \tag{18}$$

If the real part of the argument of the logarithm is negative, this term becomes very large, of the order of M_n/Γ_n, and a radiative tail arises. Further, two additional conditions must be fulfilled:

$$s \;>\; M_m^2 \qquad \text{and} \qquad \Delta = \frac{E_\gamma}{E_{\rm beam}} \;>\; 1 - \frac{M_m^2}{s} \tag{19}$$

The radiative tail has very important implications in the search for Z' effects. It is known that it enhances the Standard Model cross sections by a factor of 2–3, thus completely diluting the small signals of a Z'. Note that there are no tail effects from the Z' at energies below the Z' peak which could enhance these signals. In order to remove the Z boson tail, a cut has to be applied on the photon energy E_γ which guaranties that $\Delta = E_\gamma/E_{\rm beam} < 1 - M_Z^2/s$. This would be the case for

$$\begin{aligned} \Delta({\rm LEP200}) \;&<\; 0.792 \quad \text{i.e.} \quad E_\gamma \;<\; 79.2 \text{ GeV} \\ \Delta({\rm NLC500}) \;&<\; 0.967 \quad \text{i.e.} \quad E_\gamma \;<\; 242 \text{ GeV} \end{aligned} \tag{20}$$

After having applied this cut on the maximum photon energy, the ratio of the Z' signal to the Z boson effects remains of comparable size as it was in the Born approximation, although its numerical value is completely different. The main features of the present discussion are illustrated in Figure 2 where we plot the ratio of the hadronic cross section for the five light flavors to the muonic cross section, in the presence of a Z' of model χ [which coincides with the LR model with $\alpha_{LR} = \sqrt{2/3}$ as discussed previously] with a mass $M_{Z'} = 750$ GeV. We see that a cut on the photon energy strongly influences not only the cross section values, but also the difference between observables with and without Z' exchange.

Let us now briefly discuss the case of the pure weak radiative corrections. Within the present context, a correct treatment of these corrections is not too problematic. One simply has to add to the available Standard Model programs a piece containing the Z' cross section[5]. Higher order corrections generated by the Z' boson [25] can be safely neglected if the mass of the latter is sufficiently large as it is assumed here. We further neglect corrections due to the enlarged Higgs sector. The Standard Model corrections are generally very small below LEP100 energies since there, the photon exchange is dominating. At LEP100, they are also

[5]Note that in the case of Z–Z' mixing [which we neglect here] the situation is more complicated but allows at least some approximate solution [26].

small if the top quark is relatively light. The situation is only slightly different at energies much larger than the weak boson masses, although the corrections rise as fast as $\ln(s/M_Z^2)$. This is illustrated in Table 2 where the contribution of the weak loop corrections is compared to the photonic corrections and to the Z' signal at different energies. At $\sqrt{s} \simeq 500$ GeV they lead to shifts of a few percent. Due to the substantial contributions of the WW and ZZ box diagrams, they become dependent on the angular acceptance cut. Although being much larger than at LEP100, their effect is small compared to the large influence of the experimental cut conditions on bremsstrahlung and also to the Z' signal which is nearly one order of magnitude larger for the present parameter settings.

Finally in the case of hadronic final states, one has to take into account QCD radiative corrections. These corrections will only change the overall normalization. In the massless quark limit in which we are interested here, they can be included by simply multiplying the Born expression of $Q_T^{\gamma,Z,Z'}$ in eqs. (13,14) by a factor $(1 + \alpha_s/\pi)$ [27]. There are no QCD corrections to $Q_{FB}^{\gamma,Z,Z'}$ in this limit.

4 Experimental situation at 500 GeV

In this section we want to consider a future e^+e^- linear collider (NLC) [28] which may provide a center of mass energy of 500 GeV. We have given arguments that such an e^+e^- collider is unlikely to become a Z' factory. Therefore, we will concentrate on the Z' propagator effects which can be detected by an extension of the precision tests of the electroweak theory performed today at LEP100 to higher energies.

To characterize the experimental situation, Table 3 gives a few typical cross-sections at 500 GeV. The hadronic cross-section is a factor ≈ 3000 smaller than at the Z peak at LEP100. Therefore, harder cuts will have to be applied against two–photon events which have a cross-section logarithmically rising with s. In addition, the W^+W^- production is comparable to $q\bar{q}$ production. Figure 3 shows the energy spectrum for the dominant processes with final state hadrons. The distribution is displayed in the variable $\Delta = 1 - s'/s$ introduced earlier, with s' calculated from the measured four vectors of the final state particles and s derived from the nominal center of mass energy. The spectrum is obtained from a simulation based on PYTHIA 5.5 [29] and a simple detector representation. In the simulation, photons radiated in the initial state are taken into account but not the effects of beamstrahlung, which differ substantially for various machine designs. To suppress the two–photon background, a cut $\Delta < 0.9$ is needed. In the previous section we have discussed that such a cut is also needed in order not to dilute the Z' signal by events from the radiative return to the Z. An optimization of this cut, which also has to take into account the beamstrahlung spectrum, has not been performed and we conservatively adopt the value $\Delta < 0.7$. Typical event rates after this cut for an integrated luminosity of 20 fb^{-1}, which we will assume for all further studies, are given in Table 4.

Column 2 of Table 5 summarizes the 1990 experimental systematics of precision measure-

ments at LEP100, which are expected to improve with statistics. Comparing these numbers to the statistics in Table 4, it can be seen that it makes sense to aim at a similar precision at NLC. The clean background situation at an e^+e^- collider allows to complement calorimetry with high precision tracking devices which might well reach an accuracy $\Delta p/p^2 < 0.5 \cdot 10^{-3}$ GeV^{-1}. Therefore, for the lepton detection, similar systematic errors as at LEP100 can be achieved. For the process $e^+e^- \to q\bar{q}$ however, the situation is different due to the high W^+W^- background. Calorimetry in combination with high resolution tracking devices allowing an easy tagging of W^+W^- events, we nonetheless attribute an accuracy of 1% to the selection efficiency for the process $e^+e^- \to q\bar{q}$. The luminosity determination is complicated by the presence of beamstrahlung, requiring a precise energy measurement for small angle Bhabha pairs. It has been studied that this is feasible, allowing an absolute luminosity measurement with an error of less than 1% [30]. Table 5, column 3 summarizes the expected systematic errors at NLC which have been taken into account.

The estimates for statistics and systematic errors suggest to base our analysis on the following variables

$$\sigma^{\rm lept}, \qquad R = \frac{\sigma^{\rm had}}{\sigma^{\rm lept}}, \qquad A_{\rm FB}^{\rm lept}$$

In our considerations the index 'lept' refers to the combination of all three lepton channels, for electrons however we only consider the s–channel. Other precision tests at LEP100 involve the $b\bar{b}$ sector, which we do not consider here due to the small statistics off-resonance relative to the sum of lepton channels. For the same reason we also do not consider the τ–polarization asymmetry. To study the benefit of longitudinal polarization, we will also indicate the effect of a precision measurement of

$$A_{\rm LR}^{\rm lept}, \qquad A_{\rm LR}^{\rm had}$$

on the results obtained. These asymmetries are equal at the Z peak but off–resonance, we expect different values for both observables, due to the $\gamma\gamma$, γZ, ... contributions which are no longer suppressed.

5 Results and discussion

5.1 Z' mass limits

If at a c.m. energy of 500 GeV still all observations happen to be consistent with the Standard Model prediction, we can derive lower bounds on the mass of an additional Z' by a comparison of the measured observables with the prediction of various models. Standard Model parameters like the top and Higgs masses and the strong coupling constant, which are needed for the calculation of radiative corrections are assumed to be known. Since we neglect the small mixing angle between Z and Z', we can concentrate on a study of the deviations of $\sigma^{\rm lept}$, $A_{\rm FB}^{\rm lept}$, R and $A_{\rm LR}$ from the Minimal Standard Model predictions as function of $M_{Z'}$ and the parameters $\cos\beta$ and α_{LR}, of E_6 and LR models respectively.

Figure 4 shows for each individual observable considered, the mass limits up to which a new E_6 motivated Z' could be excluded at the 95% confidence level, as a function of the

model parameter $\cos\beta$. Figure 5 shows the analogous limits for left-right models as a function of α_{LR}. The derivation of Z' mass limits includes the effects of QED corrections for a cut Δ <0.7 and the effects of the systematic errors in Table 5. It can be seen that the observables have a complementary behavior as a function of the model parameters $\cos\beta$ and α_{LR}. The strongest limits without longitudinal polarization can be obtained from a measurement of $R = \sigma^{\rm had}/\sigma^{\rm lept}$. Figure 6 shows the Z' mass limits when combining all observables. Without longitudinal polarization, mass limits up to 3 TeV can be reached for a Z' originating from E_6 and left-right models. From Figure 6 it can be seen that the gain in sensitivity by the availability of longitudinal polarization is rather modest for E_6 models. For left–right models, longitudinal polarization would allow to extend the Z' mass limits by up to 1.2 TeV for certain α_{LR} values. To demonstrate the effect of systematic errors the mass limits calculated from statistics only are also indicated in Figure 6. In the limit of vanishing systematics, Z' mass limits could be pushed to 4 TeV for certain model parameters.

In Figure 7 we show how the Z' exclusion limits would scale with the c.m. energy available, keeping systematic errors as in Table 5 and a constant integrated luminosity of 20 fb^{-1}. Raising the c.m. energy to 1 TeV or even 2 TeV (c.f. the study performed in Ref. [31]) allows to extend the Z' mass limits up to 5 TeV or 8 TeV, respectively.

Z' discovery limits in pp collisions at LHC range up to 5 TeV [32], depending on the luminosity assumed. The Z' could be discovered in pp collisions as a peak in the invariant mass spectrum of high energy e^+e^- pairs. Therefore pp discovery limits strongly depend on the branching ratio of the Z' into e^+e^- pairs Br($Z' \to e^+e^-$). If no Z' is found at LHC, this will exclude an area in the plane of $M_{Z'}$ and Br($Z' \to e^+e^-$). Exclusion limits obtained in e^+e^- collisions are derived from the propagator effects and mainly from the $\gamma Z'$ interference, and therefore have only a very weak dependence on the total decay width of the Z'. Therefore exclusion limits derived in e^+e^- and pp collisions would be complementary.

5.2 Distinction of models

In this subsection we assume that the Z' has been discovered in pp collisions, and we want to discuss how to elucidate the origin of this new gauge boson.

In pp collisions the number of events in the Z' invariant mass peak depends on the model parameters of the Z' and its branching ratio into electrons. Therefore further quantities are needed to obtain a statement about model parameters. The only quantity accessible there is the forward–backward asymmetry of leptons. The obvious experimental requirement for the forward–backward asymmetry is charge identification. This imposes severe requirements to their tracking capabilities and probably will be limited to $M_{Z'}$ <1 TeV [33].

At a 500 GeV e^+e^- machine, we can use all observables which potentially provide mass limits on the Z' also for the identification of its origin. Let us suppose that we know that $M_{Z'}$=1 TeV and the observations are consistent with the E_6 prediction for a certain value of $\cos\beta$. Figure 7 shows as function of $\cos\beta$, which values of the model parameter α_{LR} in left-right models can be excluded at the 95% confidence level, separately for the observables

$\sigma^{\rm lept}$, $R = \sigma^{\rm had}/\sigma^{\rm lept}$ and $A_{\rm FB}^{\rm lept}$. In this figure and subsequent ones, the range of α_{LR} values which can be excluded at the 95% confidence level is indicated as white areas. Contrary the hatched areas show the regions of confusion. Combining all three observables, only the tiny hatched area in Figure 9a remains. If longitudinal polarization could be made available as well, even this tiny region of confusion would vanish for $M_{Z'}$=1 TeV. Figure 9b–d show the distinction between E_6 and left-right models for higher Z' masses. In each figure, the hatched area corresponds to the region of confusion without longitudinal polarization, the smaller cross-hatched area shows the gain of combining the statistical significance of $\sigma^{\rm lept}$, $R = \sigma^{\rm had}/\sigma^{\rm lept}$ and $A_{\rm FB}^{\rm lept}$ with that of $A_{\rm LR}^{\rm lept}$ and $A_{\rm LR}^{\rm had}$. Irrespective of the availability of longitudinal polarization, an excellent distinction between E_6 and left-right models can be obtained in the Z' mass range up to 1.5 TeV. Some discrimination can still be achieved for Z' masses up to 2 TeV. In all cases, longitudinal polarization is valuable and would allow to extend the capability to distinguish between E_6 and left-right models up to Z' masses of about 2.5 TeV.

Having discussed the distinction between different classes of models we now turn to the determination of the model parameter itself, using as an example $\cos\beta$ related to E_6 models. Figure 10 displays the result of this study for Z' masses from 1 to 3 TeV. For $M_{Z'}$ known, and data being consistent with a certain central value of $\cos\beta$ indicated on the abscissa, the ordinate gives the 1σ range for $\cos\beta$. Especially for higher Z' masses, this 1σ range may separate into disconnected regions. As in Figure 11, the hatched area refers to the combination of observables without longitudinal polarization, the smaller cross-hatched area demonstrates the benefit from including $A_{\rm LR}^{\rm lept}$ and $A_{\rm LR}^{\rm had}$. It can be seen that data could restrict the model parameter $\cos\beta$ up to Z' masses of 3 TeV.

6 Conclusions

In this article, we have shown that a 500 GeV next generation linear collider provides an interesting environment for precision tests of the Standard Model. We have performed a detailed study of radiative corrections, and shown that they are responsible for effects, which are even more pronounced than at the Z peak.

A heavy Z', even if its mass is substantially higher than the center of mass energy available in e^+e^- collisions, would manifest itself at tree level by its propagator effects [and mainly via its interference with the photon exchange diagram] producing sizeable effects on the observables $\sigma^{\rm lept}$, R=$\sigma^{\rm had}/\sigma^{\rm lept}$, $A_{\rm FB}^{\rm lept}$ and $A_{\rm LR}$. If all observables still confirm the Minimal Standard Model prediction at a center of mass energy of 500 GeV, a Z' could be excluded at the 95% confidence level up to masses of 3 TeV without, and 3.5 TeV with the availability of longitudinal polarization.

If a Z' in the mass range up to 3 TeV were to be discovered in pp collisions, an e^+e^- collider with a center of mass of mass energy of 500 GeV could give valuable contributions to its detailed investigation: the distinction between different classes of models and the deter-

mination of model parameters. In this context also longitudinal polarization could be an important tool.

Acknowledgements

We thank W. Buchmüller, M. Drees, C. Greub, J. Hewett, T. G. Rizzo and P. M. Zerwas for discussions. One of us (C. V.) wishes to thank the Swiss National Foundation (SNF) for financial support during his stay at ETH. Two of us (A. L. and T. R.) would like to thank the DESY Theory Group for hospitality where part of this work was performed.

References

[1] S. L. Glashow, *Nucl. Phys.* **B422** (1961) 579;
A. Salam, in: *Elementary Particle Theory*, ed. N. Svartholm, (1968) 367;
S. Weinberg, *Phys. Rev. Letters* **19** (1967) 1264.

[2] J. Ellis, S. Kelley and D.V. Nanopoulos, *Phys. Letters* **B249** (1990) 441 and CERN–TH. 6140/91 (1991);
U. Amaldi, W. de Boer and H. Furstenau, *Phys. Letters* **B260** (1991) 447;
P. Langacker and M. Luo, *Phys. Rev.* **D44** (1991) 817.

[3] See for example D. London and J. L. Rosner, *Phys. Rev.* **D34** (1986) 1530 and references therein.

[4] H. Georgi and S. L. Glashow, *Phys. Rev. Letters* **32** (1974) 438.

[5] For a complete review, see R. W. Robinett and J. L Rosner, *Phys. Rev.* **D25** (1982) 3036.

[6] For a detailed analysis and early references, see J. Hewett and T. G. Rizzo, *Phys. Reports* **183** (1989) 189.

[7] M. B. Green and J. H. Schwarz, *Phys. Letters* **B149** (1984) 117;
P. Candelas, G. T. Horowitz, A. Strominger and E. Witten, *Nucl. Phys.* **B258** (1985) 46;
E. Witten, *Nucl. Phys.* **B258** (1985) 75.

[8] P. Chiappetta, M. Greco et al., in: *Proceedings of the Large Hadron Collider Workshop*, Aachen, 4-9 October 1990, Vol. II, p. 685.

[9] R. M. Barnett et al., in: *Proceedings of the 1988 Snowmass Summer Study on High Energy Physics in the 1990's*, Snowmass Co., 1988;
J. Hewett and T. G. Rizzo, MAD/PH/645 (1991).

[10] J. C. Pati and A. Salam, *Phys. Rev.* **D10** (1974) 275;
For a review and references, see R. N. Mohapatra, *Unification and Supersymmetry*, Springer, New York, 1986.

[11] A. Blondel et al., *Nucl. Phys.* **B331** (1990) 293;
F. Boudjema et al., *Z. Physik* **C48** (1990) 595;
G. Belanger and S. Godfrey, *Phys. Rev.* **D34** (1986) 1309;
J. Hewett and T. G. Rizzo, *Z. Physik* **C36** (1987) 209;
V. Barger et al., *Phys. Rev.* **D35** (1987) 2893;
G. Costa et al., *Nucl. Phys.* **B297** (1988) 244;
T. G. Rizzo, ANL–HEP–CP–91–96 (Oct. 1991).

[12] Amaldi et al; *Phys. Rev.* **D36** (1987) 1385.

[13] *Workshop on e^+e^- Collisions at 500 GeV: the Physics Potential*, DESY Hamburg, Sept. 1991, Proceedings to appear (P.M. Zerwas, ed.).

[14] *Workshop on Physics and Experiments with Linear Colliders*, Saariselka, Finland, Sep. 1991, Proceedings to appear (R. Orava, ed.).

[15] P. Langacker and M. Luo, UPR–0476T (1991).

[16] J. Layssac, F. M. Renard and C. Verzegnassi, LAPP–TH–290 (1990);
G. Altarelli et al; *Phys. Letters* **B263** (1991) 459; *Phys. Letters* **B261** (1991) 146; *Nucl. Phys.* **B342** (1990) 15;
T. G. Rizzo, MAD/PH/626 (1990);
F. Del Aguila, M. Quiros and W. Hollik, CERN–TH. 6184/91 (1991);
M. C. Gonzalez–Garcia and J.W.F. Valle, *Phys. Letters* **B259** (1991) 365.

[17] see e.g. A. Djouadi et al., *Nucl. Phys.* **B349** (1991) 48.

[18] A. Chiappinelli and C. Verzegnassi, LAPP–TH–333–91 (1991).

[19] L. S. Durkin and P. Langacker, *Phys. Letters* **B166** (1986) 436.

[20] P. Langacker and S. Uma Sankar, *Phys. Rev.* **D40** (1989) 1569;
G. Beall, M. Bander and I. Soni, *Phys. Rev. Letters* **48** (1982) 848.

[21] A. Leike, Fortran code ZCAMEL, unpublished.

[22] A. Leike, T. Riemann and M. Sachwitz, *Phys. Letters* **B241** (1990) 267;
A. Leike and T. Riemann, *Z. Physik* **C51** (1991) 113.

[23] G. Bonneau and F. Martin, *Nucl. Phys.* **B27** (1971) 381;
M. Greco, G. Pancherivi and Y. Srivastava, *Nucl. Phys.* **B101** (1975) 11; *Nucl. Phys.* **B171** (1980) 118; erratum: **B197** (1982) 543.

[24] D. Bardin et al., *Phys. Letters* **B229** (1989) 405; *Nucl. Phys.* **B351** (1991) 1;
W. Beenakker, F.A. Berends and W.L. van Neerven, in: *Proceedings of the Int. Workshop on Radiative Corrections for e^+e^- Collisions*, Ringberg, ed. J.H. Kühn, (Springer, Berlin, 1989), p. 3.

[25] G. Degrassi and A. Sirlin, *Phys. Rev.* **D40** (1989) 3066.

[26] A. Leike, S. Riemann and T. Riemann, Univ. München prepr. LMU-91/06 (1991) and Fortran code ZEFIT⊕ZFITTER.

[27] J. Jersak, E. Laermann and P. Zerwas, *Phys. Rev.* **D25** (1982) 1218;
D. Bardin, O. Fedorenko and T. Riemann, JINR Dubna E2-87-663 (1987);
A. Djouadi, Z. Physik **C39** (1988) 561.
A. Djouadi, J. H. Kühn and P. M. Zerwas, *Z. Physik* **C46** (1990) 411.

[28] See machine section in [14].

[29] H.-U. Bengtsson and T. Sjostrand, *The Lund Monte Carlo for Hadronic Processes*, PYTHIA version 5.5.

[30] D.J. Miller, Luminosity studies in [13].

[31] *Proceedings of the Workshop on Physics at Future Accelerators*, La Thuile and Geneva, 7-13 January, 1987, CERN 87-07 (1987).

[32] M.C. Gonzales-Garcia and J.W.F. Valle in [8], p. 689.

[33] P. Camarri, V. Cavasinni and C.E. Wulz in [8], p. 704.

APPENDIX

In this Appendix, we give the expression of the differential cross section for the process $e^+(P^+)e^-(P^-) \longrightarrow f\bar{f}$, where $P^\pm$ are the longitudinal ($P_L^\pm$) and transverse ($P_\perp^\pm$) polarizations of the initial leptons, as well as the definition and the expressions of the various observables which have been used in the analysis.

The differential cross section $\mathrm{d}\sigma/\mathrm{d}\Omega$, with $\mathrm{d}\Omega = \mathrm{d}(\cos\theta)\mathrm{d}\phi$ the polar and azimuthal angles θ and ϕ specifying the direction of the fermion f with respect to the incoming electron, can be expressed in terms of generalized charges

$$\frac{1}{\sigma_0}\frac{\mathrm{d}\sigma}{\mathrm{d}\Omega} = \frac{3N_c}{8}\beta_f\frac{1}{2\pi}\Big\{(1-P_L^-P_L^+)\Big[(1+\beta_f^2\cos^2\theta)Q_1 + (1-\beta_f^2)Q_2 + 2\beta_f\cos\theta Q_3\Big]$$
$$+(P_L^+ - P_L^-)\Big[(1+\beta_f^2\cos^2\theta)Q_4 + (1-\beta_f^2)Q_5 + 2\beta_f\cos\theta Q_6\Big] + P_\perp^-P_\perp^+\beta_f^2\sin^2\theta\cos 2\phi Q_7\Big\} \qquad (\mathbf{A}.1)$$

where N_c is a color factor, $\beta_f = (1-4m_f^2/s)^{1/2}$ the velocity of the fermion in the final state, and σ_0 the point–like QED cross section for muon pair production, $\sigma_0 = 4\pi\alpha^2/3s$. The charges Q_1–Q_7 are given by

$$\begin{aligned}
Q_1 &= \frac{1}{4}\Big[\,|Q_{LL}|^2 + |Q_{RR}|^2 + |Q_{RL}|^2 + |Q_{LR}|^2\Big] \\
Q_2 &= \frac{1}{2}\mathrm{Re}\;[\,Q_{LL}Q_{RL}^* + Q_{RR}Q_{LR}^*] \\
Q_3 &= \frac{1}{4}\Big[\,|Q_{LL}|^2 + |Q_{RR}|^2 - |Q_{RL}|^2 - |Q_{LR}|^2\Big] \\
Q_4 &= \frac{1}{4}\Big[\,|Q_{LL}|^2 + |Q_{RL}|^2 - |Q_{RR}|^2 - |Q_{LR}|^2\Big] \\
Q_5 &= \frac{1}{2}\mathrm{Re}\;[\,Q_{LL}Q_{RL}^* - Q_{RR}Q_{LR}^*] \\
Q_6 &= \frac{1}{4}\Big[\,|Q_{LL}|^2 + |Q_{LR}|^2 - |Q_{RR}|^2 - |Q_{RL}|^2\Big] \\
Q_7 &= \frac{1}{2}\mathrm{Re}\;[\,-Q_{LL}Q_{LR}^* - Q_{RR}Q_{RL}^*]
\end{aligned} \qquad (\mathbf{A}.2)$$

For s channel gauge boson exchange the helicity amplitudes Q_{ij} with $i,j = L,R$ are

$$Q_{ij} = Q_i^{f\gamma}Q_j^{e\gamma} + \frac{Q_i^{fZ}Q_j^{fZ}}{s_W^2c_W^2}\frac{s}{s-M_Z^2+iM_Z\Gamma_Z} + \frac{Q_i^{fZ'}Q_j^{eZ'}}{c_W^2}\frac{s}{s-M_{Z'}^2+iM_{Z'}\Gamma_{Z'}} \qquad (\mathbf{A}.3)$$

$Q_{L,R}^{f\gamma}, Q_{L,R}^{fZ}, Q_{L,R}^{fZ'}$ are the reduced couplings of the left and right–handed fermions to the gauge bosons and are displayed in Table 1a for the γ, Z, in Table 1b for a Z' of E_6 origin and in Table 1c for a LR Z'. The inclusion of other gauge bosons is straightforward. For $e^+e^- \to e^+e^-$ there is a t channel contribution and one has to add an extra piece to the helicity amplitudes [$Q^2 = \frac{1}{2}s/(1-\beta_f\cos\theta)$]

$$Q_{ij} \to Q_{ij} - \left[Q_i^{e\gamma}Q_j^{e\gamma}\frac{s}{Q^2} + \frac{Q_i^{eZ}Q_j^{eZ}}{s_W^2c_W^2}\frac{s}{Q^2+M_Z^2} + \frac{Q_i^{eZ'}Q_j^{eZ'}}{c_W^2}\frac{s}{Q^2+M_{Z'}^2}\right] \qquad (\mathbf{A}.4)$$

We now give the expression for the total cross section as well as the definition of and the expressions $[f \neq e]$ for the various polarized and non polarized asymmetries. For the light fermions it is more convenient to use the formulae in the limit of vanishing fermion masses which are also given.

The production cross section normalized to σ_0:

$$\begin{aligned} R^{(f)} = \frac{\sigma(e^+e^- \to f\bar{f})}{\sigma_0} &= \frac{3}{4} N_c \beta \left[(1 + \frac{1}{3}\beta^2) Q_1 + (1-\beta^2) Q_2 \right] \\ &\longrightarrow N_c Q_1 \qquad\qquad \text{for } \sqrt{s} \gg m_f \end{aligned} \tag{A.5}$$

The unpolarized forward–backward asymmetry $A_{FB}^{(f)}$:

$$A_{FB}^{(f)} = \frac{\int_0^{2\pi} \mathrm{d}\phi \left[\int_0^1 \mathrm{d}(\cos\theta) \mathrm{d}\sigma/\mathrm{d}\Omega(\mathrm{P}^- = \mathrm{P}^+ = 0) \; - \; \int_{-1}^0 \mathrm{d}(\cos\theta) \mathrm{d}\sigma/\mathrm{d}\Omega(\mathrm{P}^- = \mathrm{P}^+ = 0) \right]}{\int_0^{2\pi} \mathrm{d}\phi \left[\int_0^1 \mathrm{d}(\cos\theta) \mathrm{d}\sigma/\mathrm{d}\Omega(\mathrm{P}^- = \mathrm{P}^+ = 0) \; + \; \int_{-1}^0 \mathrm{d}(\cos\theta) \mathrm{d}\sigma/\mathrm{d}\Omega(\mathrm{P}^- = \mathrm{P}^+ = 0) \right]}$$

$$= \frac{\beta Q_3}{(1 + \frac{1}{3}\beta^2) Q_1 + (1-\beta^2) Q_2} \xrightarrow{\sqrt{s} \gg m_f} \frac{3}{4} \frac{Q_3}{Q_1} \tag{A.6}$$

The left–right asymmetry for longitudinally polarized electron beams $A_{LR}^{(f)}$:

$$A_{LR}^{(f)} = \frac{\int \mathrm{d}\Omega \left[\mathrm{d}\sigma/\mathrm{d}\Omega(\mathrm{P}^+ = 0, \mathrm{P}_\mathrm{L}^- = -1) \; - \; \mathrm{d}\sigma/\mathrm{d}\Omega(\mathrm{P}^+ = 0, \mathrm{P}_\mathrm{L}^- = +1) \right]}{\int \mathrm{d}\Omega \left[\mathrm{d}\sigma/\mathrm{d}\Omega(\mathrm{P}^+ = 0, \mathrm{P}_\mathrm{L}^- = -1) \; + \; \mathrm{d}\sigma/\mathrm{d}\Omega(\mathrm{P}^+ = 0, \mathrm{P}_\mathrm{L}^- = +1) \right]}$$

$$= \frac{(1 + \frac{1}{3}\beta^2) Q_4 + (1-\beta^2) Q_5}{(1 + \frac{1}{3}\beta^2) Q_1 + (1-\beta^2) Q_2} \xrightarrow{\sqrt{s} \gg m_f} \frac{Q_4}{Q_1} \tag{A.7}$$

The polarized forward–backward asymmetry:

$$A_{FB,LR}^{(f)} = \frac{\int \mathrm{d}\phi \left[\int_0^1 \mathrm{d}(\cos\theta) \mathrm{d}\sigma/\mathrm{d}\Omega(\mathrm{P}_\mathrm{L}^- = -1) \; - \; \int_{-1}^0 \mathrm{d}(\cos\theta) \mathrm{d}\sigma/\mathrm{d}\Omega(\mathrm{P}_\mathrm{L}^- = +1) \right]}{\int \mathrm{d}\phi \left[\int_0^1 \mathrm{d}(\cos\theta) \mathrm{d}\sigma/\mathrm{d}\Omega(\mathrm{P}_\mathrm{L}^- = -1) \; + \; \int_{-1}^0 \mathrm{d}(\cos\theta) \mathrm{d}\sigma/\mathrm{d}\Omega(\mathrm{P}_\mathrm{L}^- = +1) \right]}$$

$$= \frac{\beta Q_6}{(1 + \frac{1}{3}\beta^2) Q_1 + (1-\beta^2) Q_2} \xrightarrow{\sqrt{s} \gg m_f} \frac{3}{4} \frac{Q_6}{Q_1} \tag{A.8}$$

The azimuthal asymmetry for transversally polarized electron beams $A_\perp^{(f)}$:

$$A_\perp^{(f)} = \frac{2}{P_\perp^- P_\perp^+} \frac{\int \mathrm{d}\Omega \left[\mathrm{d}\sigma/\mathrm{d}\Omega(\mathrm{P}_\mathrm{L}^- = \mathrm{P}_\mathrm{L}^+ = 0) \cos 2\phi \right]}{\int \mathrm{d}\Omega \left[\mathrm{d}\sigma/\mathrm{d}\Omega(\mathrm{P}_\mathrm{L}^- = \mathrm{P}_\mathrm{L}^+ = 0) \right]}$$

$$= \frac{2}{3}\beta^2 \frac{Q_7}{(1 + \frac{1}{3}\beta^2) Q_1 + (1-\beta^2) Q_2} \xrightarrow{\sqrt{s} \gg m_f} \frac{1}{2} \frac{Q_7}{Q_1} \tag{A.9}$$

a)

f	$Q_L^{f\gamma} = Q_R^{f\gamma} = e^f$	$Q_L^{fZ} = I_{3L}^f - e^f s_W^2$	$Q_R^{fZ} = -e^f s_W^2$
ν	0	$\frac{1}{2}$	$\frac{1}{2}$
e	-1	$-\frac{1}{2} + s_W^2$	s_W^2
u	$\frac{2}{3}$	$\frac{1}{2} - \frac{2}{3}s_W^2$	$-\frac{2}{3}s_W^2$
d	$-\frac{1}{3}$	$-\frac{1}{2} + \frac{1}{3}s_W^2$	$\frac{1}{3}s_W^2$

b)

f	$Q_L^{fZ'}$	$Q_R^{fZ'}$
ν	$\frac{3}{2\sqrt{6}}\cos\beta + \frac{\sqrt{10}}{12}\sin\beta$	0
e	$\frac{3}{2\sqrt{6}}\cos\beta + \frac{\sqrt{10}}{12}\sin\beta$	$\frac{1}{2\sqrt{6}}\cos\beta - \frac{\sqrt{10}}{12}\sin\beta$
u	$-\frac{1}{2\sqrt{6}}\cos\beta + \frac{\sqrt{10}}{12}\sin\beta$	$\frac{1}{2\sqrt{6}}\cos\beta - \frac{\sqrt{10}}{12}\sin\beta$
d	$-\frac{1}{2\sqrt{6}}\cos\beta + \frac{\sqrt{10}}{12}\sin\beta$	$-\frac{3}{2\sqrt{6}}\cos\beta - \frac{\sqrt{10}}{12}\sin\beta$

c)

f	$Q_L^{fZ'}$	$Q_R^{fZ'}$
ν	$\frac{1}{2\alpha_{LR}}$	0
e	$\frac{1}{2\alpha_{LR}}$	$\frac{1}{2\alpha_{LR}} - \frac{\alpha_{LR}}{2}$
u	$-\frac{1}{6\alpha_{LR}}$	$-\frac{1}{6\alpha_{LR}} + \frac{\alpha_{LR}}{2}$
d	$-\frac{1}{6\alpha_{LR}}$	$-\frac{1}{6\alpha_{LR}} - \frac{\alpha_{LR}}{2}$

Table 1: Left–handed and right–handed couplings of Standard Model fermions to the gauge bosons as defined in eq. (3):
a) couplings to the photon and the Z boson as defined in eq. (4).
b) couplings to the Z' in E_6 models as a function of the parameter $\cos\beta$.
c) couplings to the Z' in left–right models as a function of the parameter α_{LR}.

$\sigma_{\mu\mu}$ [pb] vs. $\sqrt{s}$ [GeV]	91.18	200	500
brems. + run. α	1487	8.198	1.342
with a cut	1190	2.627	0.3861
with a Z'	1190	2.586	0.3376
with weak cor.	1185	2.592	0.3429
with $m_t = 200$ GeV	1189	2.634	0.3487

Table 2: Cross section for muon pair production at different c.m. energies. We use the parameter values: $M_Z = 91.18$ GeV, $m_t = 90$ GeV, M_H =300 GeV, $M_{Z'} = 1$ TeV and $\theta_{\rm mix} = 0$. We take $s'_{\rm min} = 0.3s$ and $150° \leq \theta \leq 30°$. The different contributions are varied/included step by step.

process	cross-section [pb]
$e^+e^- \to q\bar{q}$	11.5
$e^+e^- \to \mu^+\mu^-$	1.1
$e^+e^- \to t\bar{t} \quad (m_t = 120$ GeV$)$	0.8
$e^+e^- \to W^+W^-$	8.0
$e^+e^- \to e^+e^-W^+W^-$	0.2
$e^+e^- \to e\nu WZ$	0.02
$e^+e^- \to e^+e^-q\bar{q} \quad (M_{q\bar{q}} > 20$ GeV$)$	33.5

Table 3: e^+e^- cross-sections at a c.m. energy of 500 GeV.

process	statistics
$e^+e^- \to l^+l^-$	$26 \cdot 10^3$
(s–channel $e^+e^- + \mu^+\mu^- + \tau^+\tau^-$)	
$e^+e^- \to q\overline{q}$	$52 \cdot 10^3$
$e^+e^- \to W^+W^-$	$59 \cdot 10^3$
$e^+e^- \to e^+e^-q\overline{q}$	$0.1 \cdot 10^3$

Table 4: Typical event statistic at a c.m. energy of 500 GeV based on an integrated luminosity of 20 pb^{-1}. The statistics includes the efficiency for a cut $\Delta < 0.7$.

systematics	LEP 1990	NLC
event selection:		
$\frac{\Delta\epsilon_\mu}{\epsilon_\mu}$	$\geq 0.5\%$	0.5%
$\frac{\Delta\epsilon_{had}}{\epsilon_{had}}$	0.2–0.4%	1%
lepton FB-asymmetry	negl.	negl.
absolute luminosity	0.7–0.9%	$\leq$1%
$\Delta A_{\rm LR}$	0.003	0.003

Table 5: Systematic errors for precision measurements at LEP100 and at NLC.

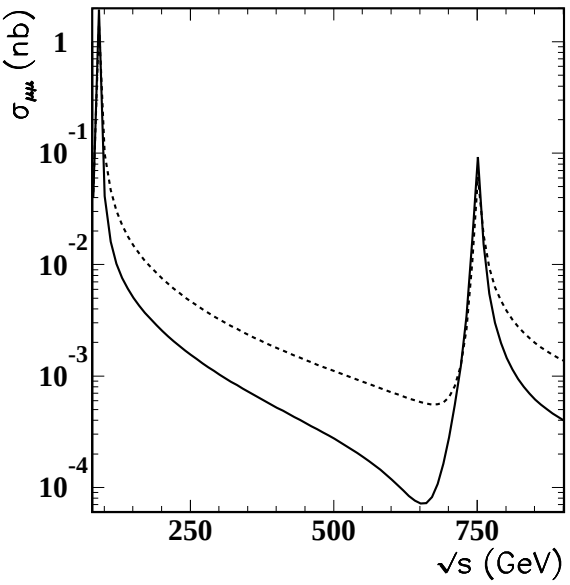

Figure 1: The total cross section for muon pair production $\sigma^{\mu\mu}$ as a function of the c.m. energy in the presence of a Z'_χ with a mass $M_{Z'} = 750$ GeV. Shown are the Born approximation (solid curve) and the QED corrected cross sections [without a cut on the photon energy] (dashed curve).

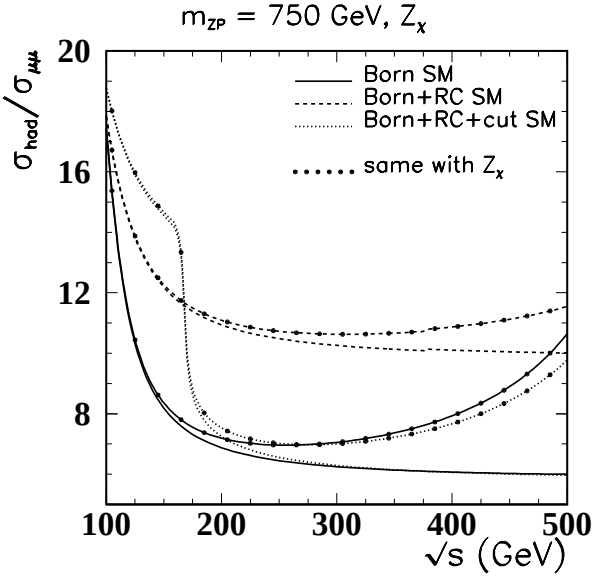

Figure 2: The ratio of hadronic and muonic cross sections $R = \sigma^{\rm had}/\sigma^{\mu\mu}$ as a function of the c.m. energy with and without a Z'_χ with a mass $M_{Z'} = 750$ GeV (dotted lines). Shown are the Born approximation (solid curves), including QED corrections without a cut on the photon energy (dashed curves) and with a cut (dotted curves).

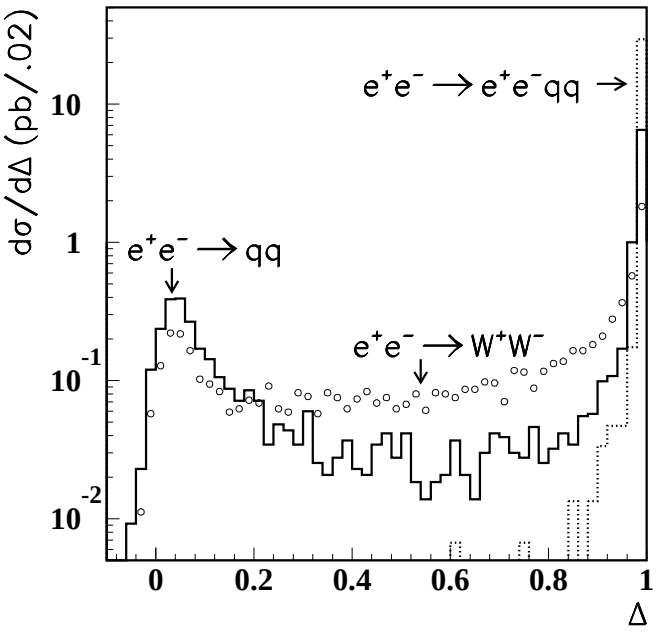

Figure 3: Final state energy spectrum for the dominant processes with final state hadrons at an e^+e^- collider with a c.m. energy of 500 GeV. The final state energy is expressed in the variable Δ=1-s'/s, with s' calculated from the measured four vectors of the final state particles and s derived from the nominal center of mass energy. The spectrum is obtained from a simulation based on PYTHIA 5.5 [29] and a simple detector representation. In the simulation effects of initial state radiation are taken into account, but not the effects of beamstrahlung.

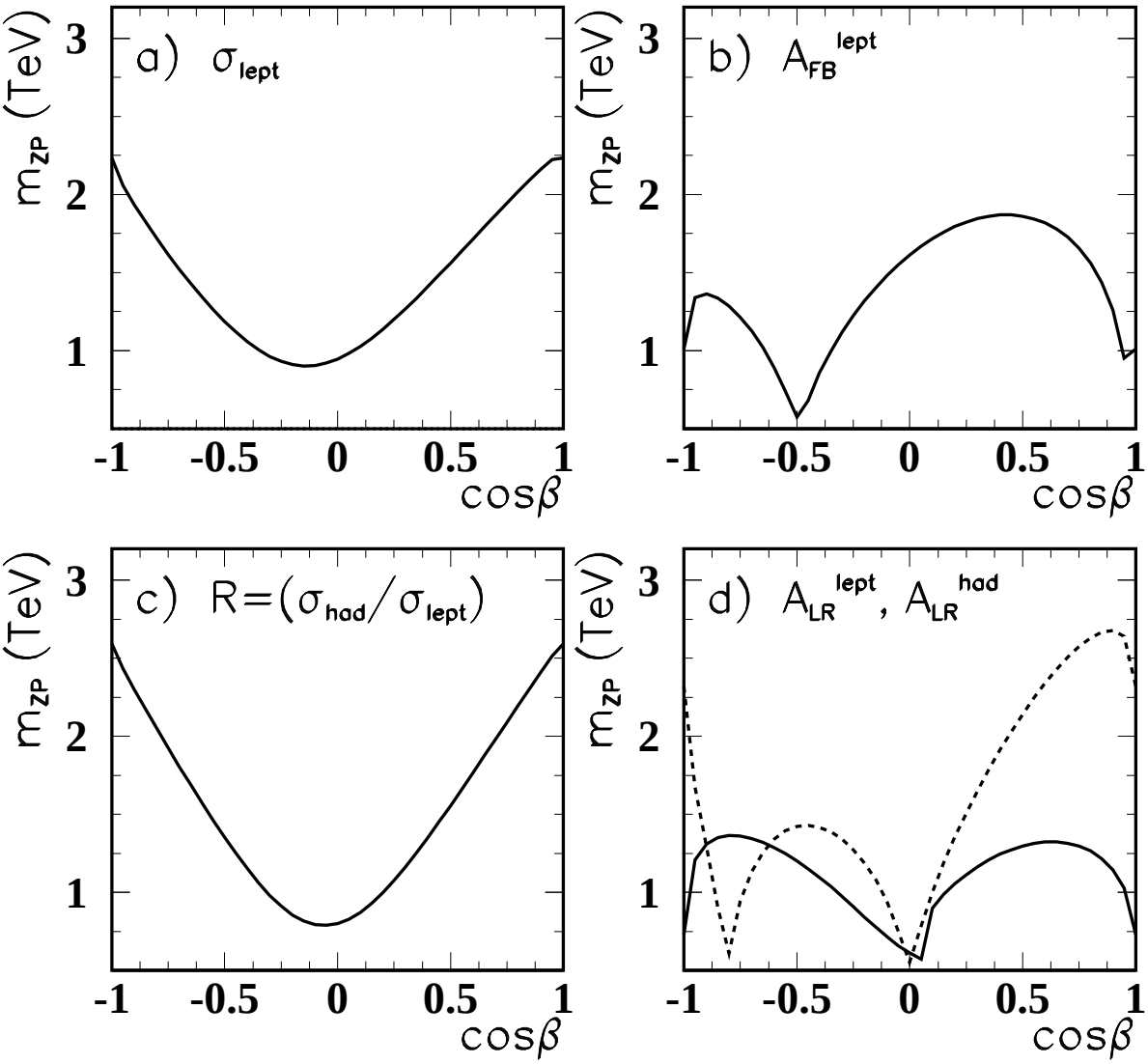

Figure 4: Z' mass limits in E_6 models as function of the parameter $\cos\beta$. Shown are 95% confidence limits based on an integrated luminosity of 20 fb^{-1} at a c.m. energy of 500 GeV. Radiative corrections, a cut on the final state fermion energy of $\Delta = 1 - s'/s < 0.7$ and experimental systematics have been taken into account.
a) From the leptonic cross-section $\sigma^{\rm lept}$.
b) From the lepton forward backward asymmetry $A_{\rm FB}^{\rm lept}$.
c) From the ratio of the hadronic and leptonic cross-sections R=$\sigma^{\rm had}/\sigma^{\rm lept}$.
d) From the polarisation asymmetry $A_{\rm LR}^{\rm had}$ (solid curve) and $A_{\rm LR}^{\rm lept}$ (dashed curve).

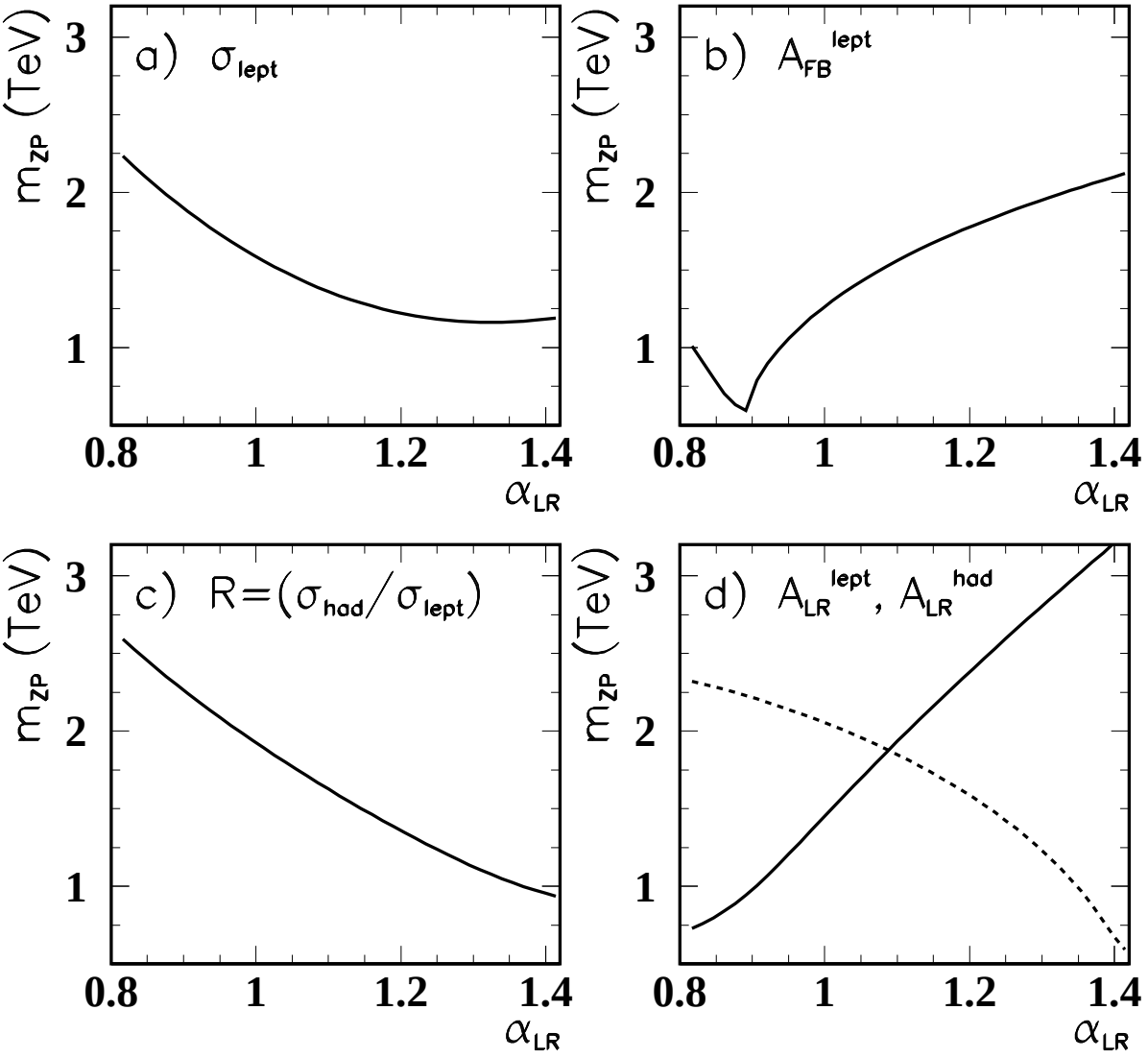

Figure 5: Z' mass limits in left-right models as function of the parameter α_{LR}. Shown are 95% confidence limits based on an integrated luminosity of 20 fb^{-1} at a c.m. energy of 500 GeV. Radiative corrections, a cut on the final state fermion energy of $\Delta = 1 - s'/s < 0.7$ and experimental systematics have been taken into account.
a) From the leptonic cross-section $\sigma^{\rm lept}$.
b) From the lepton forward backward asymmetry $A_{\rm FB}^{\rm lept}$.
c) From the ratio of the hadronic and leptonic cross-sections R=$\sigma^{\rm had}/\sigma^{\rm lept}$.
d) From the polarisation asymmetry $A_{\rm LR}^{\rm had}$ (solid curve) and $A_{\rm LR}^{\rm lept}$ (dashed curve).

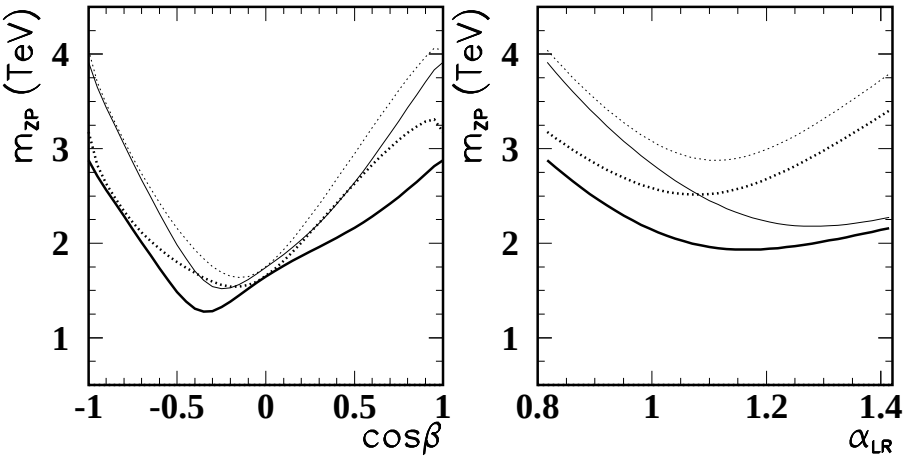

Figure 6: Z' mass limits in E_6 and left-right models as function of the parameters $\cos\beta$ and α_{LR}, respectively. Shown are 95% confidence limits based on an integrated luminosity of 20 fb^{-1} at a c.m energy of 500 GeV. Radiative corrections, a cut on the final state fermion energy of $\Delta = 1 - s'/s < 0.7$ and experimental systematics have been taken into account. The thick solid curve results from combining the significance of a measurement of $\sigma^{\rm lept}$,R=$\sigma^{\rm had}/\sigma^{\rm lept}$ and $A_{\rm FB}^{\rm lept}$. The thick dotted curve assumes that longitudinal polarization can be made available and includes the measurement of $A_{\rm LR}^{\rm had}$ and $A_{\rm LR}^{\rm lept}$. The corresponding thin curves only include the effects of statistics.

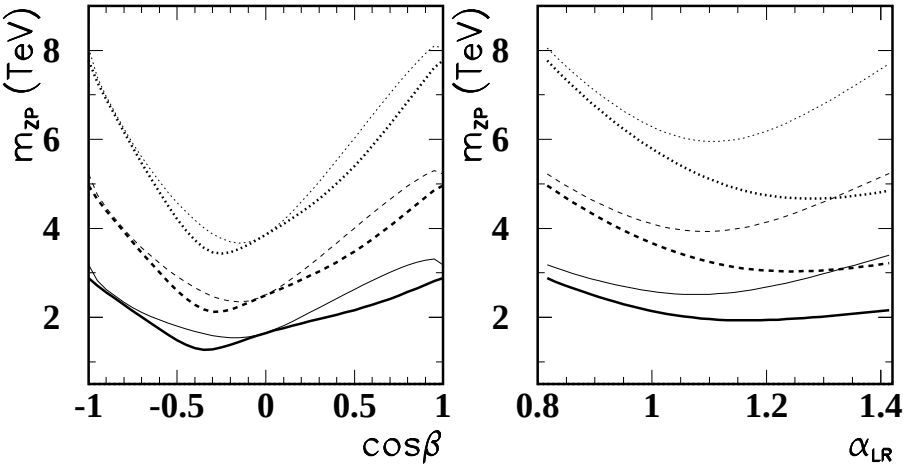

Figure 7: Z' mass limits in E_6 and left-right models as function of the parameter $\cos\beta$ and α_{LR}, respectively. Shown are 95% confidence limits for a c.m. energy of 0.5 TeV (solid lines), 1.0 TeV (dashed lines) and 2.0 TeV (dotted lines), respectively. Integrated luminosity and experimental accuracies are the same as for Figures 4–6. The lower thick curves result from combining the significance of a measurement of $\sigma^{\rm lept}$,R=$\sigma^{\rm had}/\sigma^{\rm lept}$ and $A_{\rm FB}^{\rm lept}$. The upper thin curves include the measurement of $A_{\rm LR}^{\rm had}$ and $A_{\rm LR}^{\rm lept}$.

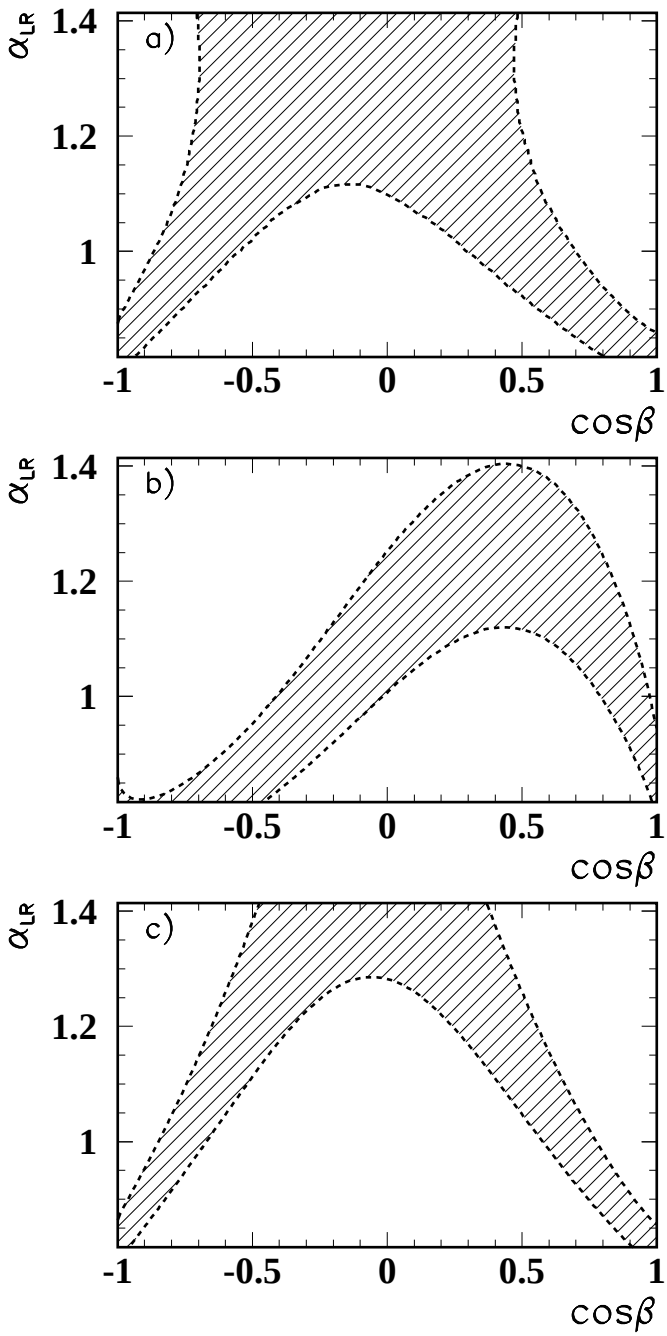

Figure 8: Distinction between E_6 and left-right models for a Z' mass of 1 TeV. Integrated luminosity, c.m. energy and experimental accuracies are the same as for Figures 4–6. Shown is the range of the parameter α_{LR} in left-right models which can be excluded at the 95% confidence level, if the experimental observations are consistent with a certain value of $\cos\beta$. The exclusion range is indicated as white area, the hatched area denotes the region of confusion.
a) Distinction of models from the leptonic cross-section $\sigma^{\rm lept}$.
b) Distinction of models derived from the lepton forward backward asymmetry $A_{\rm FB}^{\rm lept}$.
c) Distinction of models derived from the ratio R=$\sigma^{\rm had}/\sigma^{\rm lept}$.

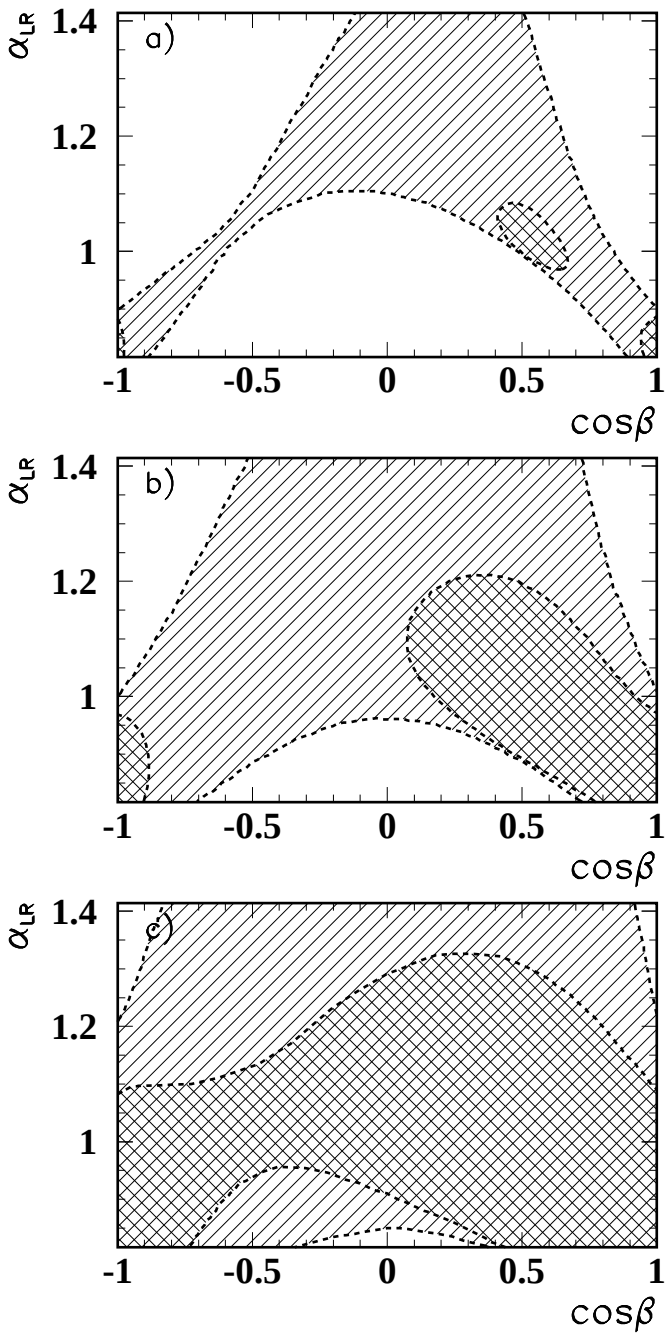

Figure 9: Distinction between E_6 and left-right models when combining the significance of $\sigma^{\rm lept}$, $A_{\rm FB}^{\rm lept}$ and R=$\sigma^{\rm had}/\sigma^{\rm lept}$ for increasing Z' masses (a) $M_{Z'}$=1.5 TeV, b) $M_{Z'}$=2 TeV and c) $M_{Z'}$=2.5 TeV). Integrated luminosity, c.m. energy and experimental accuracies are the same as for Figures 4–6. If all observations are consistent with the E_6 prediction for a certain value of cos β then the white areas indicate which values of the parameter α_{LR} in left-right models can be excluded at the 95% confidence level. The exclusion range is indicated as white area, the hatched area denotes the region of confusion. The smaller cross-hatched area shows the gain in sensitivity, if longitudinal polarization can be made available, providing in addition a measurement of $A_{\rm LR}^{\rm lept}$ and $A_{\rm LR}^{\rm had}$.

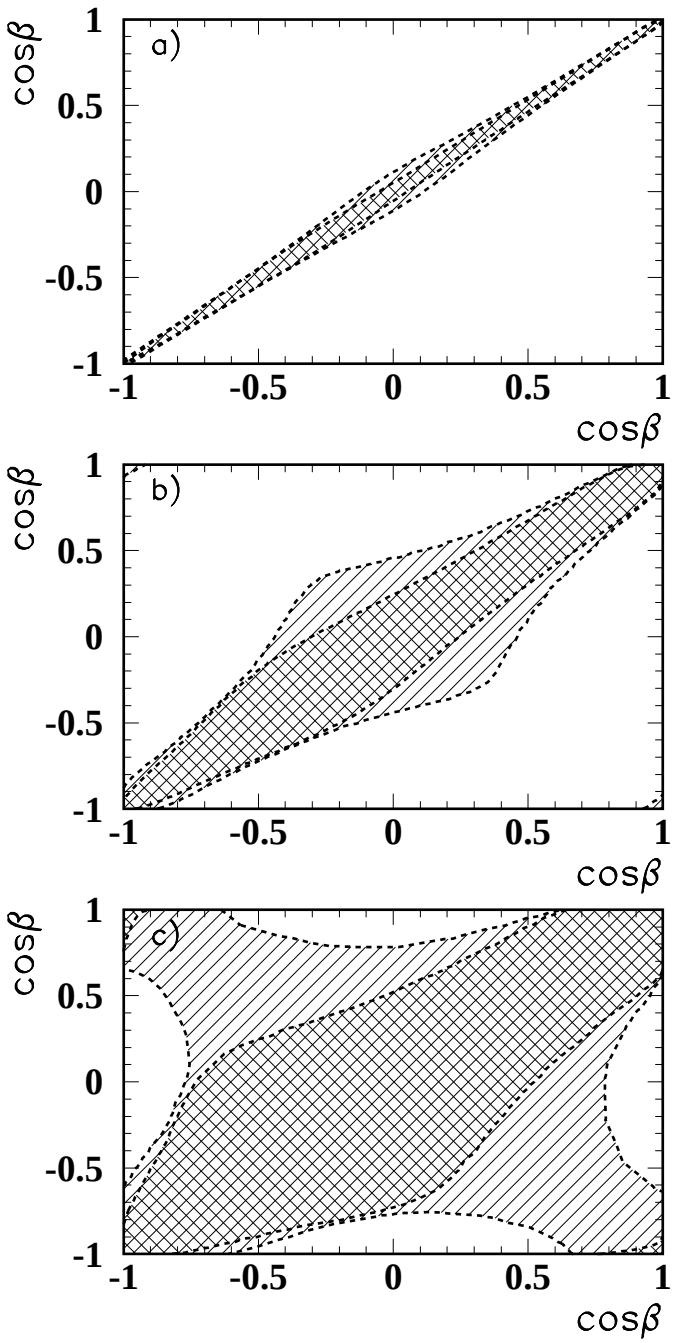

Figure 10: Determination of the E_6 model parameter $\cos\beta$ for increasing Z' masses (a) $M_{Z'}$=1 TeV, b) $M_{Z'}$=2 TeV and c) $M_{Z'}$=3 TeV). Integrated luminosity, c.m. energy and experimental accuracies are the same as for Figures 4–6. For $M_{Z'}$ known, and data being consistent with the E_6 prediction for a certain central value of $\cos\beta$ indicated on the abszissa, the ordinate gives the 1-σ range for $\cos\beta$. As in Figure 9 the hatched area refers to the combination of observables without longitudinal polarization, the smaller cross-hatched area demonstrates the benefit from includig $A_{\rm LR}^{\rm lept}$ and $A_{\rm LR}^{\rm had}$.